A Solution for Boundary Problems in Isentropic Coordinate Models

DENNIS G. DEAVEN

National Center for Atmospheric Research[1], Boulder, Colo. 80303

(Manuscript received 22 May 1975, in revised form 11 May 1976)

ABSTRACT

A numerical model is designed to integrate the primitive equations in two dimensions to evaluate a new vertical coordinate scheme for hydrostatic flow. Because potential temperature is nearly conserved for large-scale atmospheric flow, potential temperature is utilized as the vertical coordinate in the layer bounded by the lower troposphere and the top of the model atmosphere which is near the middle stratosphere. The vertical coordinate scheme circumvents some of the problems that have appeared in previous isentropic coordinate models by utilizing a variable depth layer near the earth's surface in which a function of pressure is the vertical coordinate. For this reason, no coordinate surface intersects the surface of the earth and complicated topographic features can easily be constructed. In addition, adiabatic and superadiabatic lapse rates can develop near the surface of the earth because the vertical coordinate in this region is a quasi-horizontal function of pressure.

Two experiments are performed to test the proposed vertical coordinate scheme. The formation of waves that appear in the atmosphere when the flow is normal to a mountain ridge is simulated by the first experiment. A temperature excess is introduced at the earth's surface for the second experiment to simulate conditions analogous to a large industrial power park.

The results of the experiments illustrate that the layer developed here can be used as the interface between an isentropic coordinate layer and the earth's surface in numerical prediction models.

1. Introduction

Isentropic processes are of considerable interest to meteorologists because potential temperature is nearly conserved for large-scale flow over much of the atmosphere.

The first law of thermodynamics for an isentropic process can be written simply and concisely as

$$\frac{d\theta}{dt}=0 \tag{1}$$

for an ideal gas. In the atmosphere, (1) is approximately satisfied except in cloud layers or in shallow layers next to the surface of the earth. For this reason the assumption of isentropic flow is justified for many large-scale atmospheric flows.

If potential temperature is utilized as the vertical coordinate, then the equations of motion are simplified considerably because, along with the hydrostatic assumption, the flow is formally horizontal with small vertical variations. When potential temperature is the vertical coordinate and the flow is isentropic, then the coordinate surfaces are material surfaces with each air parcel remaining embedded in its respective isentrope. If the flow is non-isentropic, then the vertical velocity $d\theta/dt$ is directly related to the diabatic heating rate. Although diabatic heating terms are present, the equations of motion are still simplified because over most of the atmosphere the magnitude of the diabatic heating term is small compared to the vertical velocity.

The isentropic assumption leads to considerable simplification in numerical models because it eliminates the problem of incompatible vertical and horizontal scales affecting computational accuracy and truncation. In addition, the variable resolution of the isentropic coordinate system with automatically increased vertical resolution in regions of increased stability provides a supplementary benefit to a numerical model in which computer storage is limited.

These benefits, however, are offset by three serious problems that have appeared in previous isentropic coordinate models. The first problem is caused by diabatic heating or breaking waves, either of which can produce adiabatic or even superadiabatic lapse rates and a failure of the coordinate transformation. The second problem is correctly modeling the behavior of the isentropes that intersect the surface of the earth. The third problem, which is related to the second, concerns representation of complicated terrain features in a model in which the information surfaces have a variable altitude.

It is reasonable to say, that despite development of simple isentropic coordinate models and primitive ex-

[1] The National Center for Atmospheric Research is sponsored by the National Science Foundation.

perimentation with the behavior of intersection surfaces in such models, all of these problems have been an effective barrier to their development as either general circulation models or as operational prediction models. The efficacy of any numerical model simulating the atmosphere is directly dependent upon the ability of the model to simulate the many complex processes that occur in the planetary boundary layer.

For the reasons mentioned before, potential temperature cannot be used as the vertical coordinate in the planetary boundary layer. In this paper, a numerical technique is developed to include topographic features and surface heating in a primitive equation model in which potential temperature is the vertical coordinate over the majority of the domain. Results show that the approach can be applied in development of either global circulation models in isentropic coordinates (which is important for atmospheric energetics) or for synoptic or mesoscale models.

2. The numerical model

In order to show that a solution for some of the problems that have appeared in previous isentropic coordinate models has been found, the model is cast in two dimensions, with x the horizontal coordinate and θ (potential temperature) the vertical coordinate (Deaven, 1974). The two-dimensional flow approximation allows the degree of vertical resolution that is necessary to properly model the vertical flux of sensible heat and momentum in the boundary layer and free atmosphere. Also, computer time and storage requirements are minimized by this procedure.

The vertical structure of the hydrostatic model is divided into two distinct subregions: an upper layer simulating the free atmosphere in which potential temperature is the vertical coordinate and a lower boundary layer in which sigma (Shuman and Hovermale, 1968)

$$\sigma=\frac{p-p_0}{p_s-p_0} \tag{2}$$

is the vertical coordinate. In this expression, p_0 is the pressure at the material surface interface between the sigma coordinate layer and the isentropic coordinate layer, while p_s is the surface pressure. There are 25 grid points in the vertical direction with 10 reserved for use in the boundary layer while the remaining 15 grid points form the isentropic coordinate section. Because the interface between the two coordinate systems can move up or down, vertical resolution in the lower layer varies, but usually equals about 300 m between grid points. In the isentropic region the vertical resolution varies from about 800 m between layers just above the interface to about 1600 m between layers at the top of the isentropic section near 25 mb.

In the horizontal the model is divided into three subregions: a central primary region and two buffer zones on either side of the central region. In the central region, from grid point 15 to 45, the horizontal resolution is fixed at 7 km between grid points and linear diffusion reduces the amplitude of the $2\Delta x$ wave by 2% each time step. Grid points 1–15 and 45–60 comprise the lateral boundary regions in which the horizontal grid increment varies exponentially from the 7 km value in the central region to 200 km at each edge. Within these lateral subregions the linear diffusion coefficient increases from its value in the central region to an amount large enough to eliminate the $2\Delta x$ wave as the wave nears either edge of the grid at grid points 1 or 60. The two lateral subregions act as buffers that absorb spurious small-scale oscillations generated in the central primary region. For this reason, all figures illustrating experimental results depict the central primary region only.

a. The isentropic coordinate layer

The isentropic coordinate section of the numerical model is a direct adaptation of a model proposed by Eliassen and Raustein (1968). Their two-layer model was extended to 14 layers and the surface of the earth was replaced by a material surface interface positioned above the planetary boundary layer. In addition, a parameterization scheme was included to simulate the effect of diabatic terms for a dry atmosphere.

The equations for the troposphere and lower stratosphere include (i) the two-dimensional horizontal equation of motion in isentropic coordinates

$$\frac{\partial u}{\partial t_\theta}=-u\frac{\partial u}{\partial x_\theta}-\dot{\theta}\frac{\partial u}{\partial \theta}-\frac{\partial \psi}{\partial x_\theta}+F_x+F_z, \tag{3}$$

in which F_x represents a horizontal diffusion term added for computational reasons and F_z is a parameterized vertical mixing term which is defined later, (ii) the continuity equation for hydrostatic motion

$$\frac{\partial}{\partial t}\left(\frac{\partial p}{\partial \theta}\right)=-\frac{\partial}{\partial x}\left(u\frac{\partial p}{\partial \theta}\right)-\frac{\partial}{\partial \theta}\left(\dot{\theta}\frac{\partial p}{\partial \theta}\right), \tag{4}$$

and (iii) the hydrostatic equation

$$\frac{\partial \psi}{\partial \theta}=\pi=c_p\left(\frac{p}{p_{00}}\right)^{R/c_p}, \tag{5}$$

in which ψ is the Montgomery streamfunction.

The continuity equation can be integrated downward from the upper boundary θ^* to yield a pressure tendency equation at each isentropic level:

$$\frac{\partial p}{\partial t_\theta}=\frac{\partial p}{\partial t}\bigg|_{\theta^*}+\int_\theta^{\theta^*}\frac{\partial}{\partial x}\left(u\frac{\partial p}{\partial \theta}\right)d\theta+\int_\theta^{\theta^*}\frac{\partial}{\partial \theta}\left(\dot{\theta}\frac{\partial p}{\partial \theta}\right)d\theta. \tag{6}$$

The integration of these three equations subject to

boundary and initial conditions, along with a parameterization of the heating rate, provides a powerful and economical method to describe and predict the flow in the free atmosphere. In addition, the vertical motion can be determined subsequently by expanding the total derivative of the height of each isentropic surface in the form

$$w=\frac{dh_\theta}{dt}=\frac{\partial h_\theta}{\partial t}+u\frac{\partial h_\theta}{\partial x}+\dot{\theta}\frac{\partial h_\theta}{\partial \theta}, \tag{7}$$

where

$$h_\theta=\frac{\psi-\theta\pi}{g}. \tag{8}$$

If the values of ψ and π are stored at each grid point for each time step, then the total change of h_θ can easily be approximated and w calculated at each grid point.

b. *The sigma-coordinate layer boundary layer*

Since the intersection of potential temperature surfaces with the ground is an essential feature for the dynamics of cyclones as shown by Pedlosky (1964), the troublesome intersections must be retained in any realistic numerical model. Furthermore, in the well-mixed region close to the surface of the earth, insolation may cause the potential temperature to decrease or remain constant as a function of height, which renders potential temperature useless as a vertical coordinate. For this reason a layer is constructed which permits intersections and allows the lapse rate to become greater than or equal to the adiabatic lapse rate by using a quasi-horizontal system. The layer is represented with (2) as the vertical coordinate near the surface of the earth. Therefore the value of sigma is zero at the coordinate interface and is equal to unity at the surface of the earth. Because sigma is always 1 at the earth's surface, topographic features are easily included. This layer with sigma coordinates describes the temperature distribution during periods of strong surface heating, permits surface topographic features to be included, and simplifies the surface boundary condition because $d\sigma/dt=0$ along the material surface of the earth.

The equations in the sigma-coordinate layer include the equation of motion for the u component

$$\frac{\partial u}{\partial t_\sigma}=-u\frac{\partial u}{\partial x_\sigma}-\dot{\sigma}\frac{\partial u}{\partial \sigma}-\theta\frac{\partial \pi}{\partial x_\sigma}-g\frac{\partial h_\sigma}{\partial x_\sigma}+F_x+F_z, \tag{9}$$

the thermodynamic equation

$$\frac{\partial \theta}{\partial t_\sigma}=-u\frac{\partial \theta}{\partial x_\sigma}-\dot{\sigma}\frac{\partial \theta}{\partial \sigma}+F_x+\dot{\theta}, \tag{10}$$

the continuity equation for hydrostatic motion

$$\frac{\partial}{\partial t}\left(\frac{\partial p}{\partial \sigma}\right)=-\frac{\partial}{\partial x}\left(u\frac{\partial p}{\partial \sigma}\right)-\frac{\partial}{\partial \sigma}\left(\dot{\sigma}\frac{\partial p}{\partial \sigma}\right), \tag{11}$$

the hydrostatic equation

$$\frac{\partial h_\sigma}{\partial \pi}=-\frac{\theta}{g} \tag{12}$$

and the definition of sigma [Eq. (2)].

Because $d\sigma/dt=0$ at the surface ($\sigma=1$) and at the interface ($\sigma=0$), a vertical integration of the continuity equation gives

$$\left.\frac{\partial p}{\partial t}\right|_{\sigma=1}=\left.\frac{\partial p}{\partial t}\right|_{\sigma=0}-\int_0^1\frac{\partial}{\partial x}\left(u\frac{\partial p}{\partial \sigma}\right)d\sigma \tag{13}$$

for the surface pressure tendency. The pressure tendency $\partial p/\partial t|_{\sigma=0}$ on the interface at the top of the sigma-coordinate layer is provided from the isentropic section of the model because the surface at $\sigma=0$ is the lower boundary of the isentropic coordinate section. With the pressure tendencies known at the interface and at the surface of the earth, the continuity equation can be integrated from zero to any sigma level to determine the value of $d\sigma/dt$ on each surface, i.e.,

$$\frac{d\sigma}{dt}=-\int_0^\sigma\frac{\partial u}{\partial x}d\sigma+\frac{\partial}{\partial x}\left(\frac{\partial p}{\partial \sigma}\right)\Big/\frac{\partial p}{\partial \sigma}\int_0^\sigma u d\sigma-\sigma\frac{\partial}{\partial t}\left(\frac{\partial p}{\partial \sigma}\right)\Big/\frac{\partial p}{\partial \sigma}, \tag{14}$$

where

$$\frac{\partial p}{\partial \sigma}=p_s-p_0. \tag{15}$$

These equations, the boundary and initial conditions, and a parameterization of the heating rate determine the flow in the sigma-coordinate layer.

Again, as in the isentropic-coordinate section, the vertical motion can be obtained by expanding the total derivative of the height of each sigma surface as

$$w=\frac{dh_\sigma}{dt}=\frac{\partial h_\sigma}{\partial t}+u\frac{\partial h_\sigma}{\partial x_\sigma}+\frac{d\sigma}{dt}\frac{\partial h_\sigma}{\partial \sigma}. \tag{16}$$

The top surface of the sigma-coordinate layer is initially placed at a constant pressure above the height of the planetary boundary layer. As the model boundary layer is modified by the surface heating, the top surface of the sigma-coordinate layer is free to move up or down in response to the horizontal mass flux beneath it

c. The parameterization of heat flux and subgrid-scale mixing

The eddy coefficient K_z for sensible heat and momentum transfer is defined (Deardorff, 1967) by

$$H=-\rho c_p K_z\left(\frac{\partial\theta}{\partial z}-\gamma_c\right), \tag{17}$$

where H is the vertical eddy flux of sensible heat in both the sigma-coordinate layer and the isentropic-coordinate layer. The constant γ_c adjusts the lapse rate to permit a counter-gradient heat flux.

The variation of the vertical heat flux determines the heating rate $d\theta/dt$ in the two coordinate layers by

$$\frac{d\theta}{dt}=-\frac{1}{\rho c_p}\frac{\partial H}{\partial z}, \tag{18}$$

where radiative temperature change and release of latent heat have been neglected.

The formulation of K_z adapted directly from Deardorff (1967) is

$$K_z=\begin{cases}\dfrac{K^*}{(1+c_1\,\mathrm{Ri})}, & \text{for } \dfrac{\partial\theta}{\partial z}\geqslant\gamma_c\\[2ex] K^*+c_2\left\{1-\exp\left[\alpha\left(\dfrac{\partial\theta}{\partial z}-\gamma_c\right)\right]\right\}, & \text{for } \dfrac{\partial\theta}{\partial z}<\gamma_c,\end{cases} \tag{19}$$

where Ri is an adjusted Richardson number

$$\mathrm{Ri}=\frac{g}{T}\left(\frac{\partial\theta}{\partial z}-\gamma_c\right)\Big/\left(\frac{\partial u}{\partial z}\right)^2 \tag{20}$$

and K^*, c_1, c_2 and γ_c are empirical constants.

For vanishing turbulent heat flux $\partial\theta/\partial z=\gamma_c$ and $K_z=K^*$. The constant α is given by

$$\alpha=\left.\frac{c_1 g K^*}{c_2 T\left(\dfrac{\partial u}{\partial z}\right)^2}\right|_{(\partial\theta/\partial z)=\gamma_c}, \tag{21}$$

which is evaluated at the level at which heat flux vanishes in order that $\partial K_z/\partial(\partial\theta/\partial z)$ be continuous at the height where $\partial\theta/\partial z=\gamma_c$.

The constants c_2 and K^* in Deardorff's (1967) original paper are evaluated here as a function of the thickness of each layer, i.e.,

$$K_j^*=\frac{0.20}{11}(z_{j+1}-z_j)^2/2\Delta t, \tag{22}$$

$$c_2=10\,K^*, \tag{23}$$

where the subscript j increases upward from 1 to 24 and z is the height of either a sigma surface or an isentrope. The maximum value of the eddy coefficient K_z is equal to K^*+c_2 or

$$K_{z_{\max}}=0.20(z_{j+1}-z_j)^2/2\Delta t. \tag{24}$$

A linear stability analysis of the diffusion equation indicates that the inequality

$$K_{z_{\max}}\leqslant 0.5(z_{j+1}-z_j)^2/2\Delta t \tag{25}$$

must be satisfied to preserve computational stability. The constant 0.20 in (24) was determined empirically by varying the surface heating rate in a number of experiments. If radiational cooling and latent heat release are included in the thermodynamic equation, then the constant will have to be determined, and may become a function of height, stability or cloud cover.

The calculation of the heat flux, heating rate and the eddy diffusion coefficient is accomplished in similar fashion in the isentropic-coordinate layer and the sigma-coordinate layer. If the heating rate or the heat flux is specified along the surface of the earth, then heating rates and eddy diffusion coefficients are uniquely determined at each time step for all grid points by the parameterization method.

The value of K_z as determined above is used as an eddy coefficient for the diffusion of momentum and heat. Adjustment of the ratio of $K_z^{(H)}$ for heat to $K_z^{(M)}$ for momentum could easily be included as an additional sophistication. This ratio probably would be a function of height and stability as determined from empirical or theoretical studies. However, in all experiments to be discussed here, the ratio was set equal to unity.

The parameterization of the heat flux was performed with height as the vertical coordinate to facilitate the calculation of heat flux across the coordinate interface and eliminate additional coordinate transformations.

d. The numerical integration of the equations

The numerical integration scheme used here is similar to that employed in primitive equation models. Local tendencies are computed with spatial finite differences for each prognostic variable at each grid point. Then each local tendency is extrapolated forward in time. This two-step procedure is repeated for the duration of the numerical integration.

All spatial derivatives are approximated with the modified central differences termed semi-momentum operators by Shuman (1962). These finite difference operators, in addition to conserving momentum and retaining the linear stability characteristics of a central difference operator, suppress nonlinear instability. The linear stability criterion is $(c\Delta t)\Delta x\leqslant 1$ in which c is the phase speed of the fastest traveling gravity wave ($\sim$330 m s^{-1}) in the system. During all the experiments to be discussed later, the minimum interval for Δx was 7 km and Δt was set equal to 20 s.

Temporal derivatives of all quantities, with the exception of terms involving diffusion coefficients, are approximated with finite differences that are centered in time. The diffusion terms are evaluated with forward time differences to preserve computational stability. This procedure, centered in space and time, commonly termed the leap-frog method, has the following qualities: computational stability, small truncation error, no selective amplitude damping, and moderate phase acceleration of the physical mode (Haltiner, 1971).

e. Problems at the coordinate interface

Because the integration to obtain $\partial p/\partial t_\theta$ at each isentropic surface was performed in isentropic coordinates, (6) must be transformed into sigma coordinates for later use in the sigma-coordinate layer. The coordinate transformation is

$$\frac{\partial p}{\partial t_\sigma}=\frac{\partial p}{\partial t_\theta}+\frac{\partial p}{\partial \theta}\frac{\partial \theta}{\partial t_\sigma}, \tag{26}$$

in which the subscripts θ and σ refer to the two coordinate systems. Inspection of (10) indicates that $\partial\theta/\partial t_\sigma=0$ at the interface whenever there is no variation of potential temperature along the coordinate interface and the heating rate $d\theta/dt$ is equal to zero. Therefore, if the coordinate interface is initially an isentropic surface which is above the planetary boundary layer where the heating rate is negligible, then there will be few truncation errors introduced by the coordinate transformation.

Provision is made in the computer program to allow any number of isentropic information surfaces to intersect the coordinate interface whenever the value of potential temperature on the interface exceeds the value of the isentropic information surface above it. Quantities stored at grid points on the isentropic surface that has plunged into the sigma-coordinate layer are ignored during subsequent calculations and do not enter into the finite difference calculations. Whenever the value of potential temperature at a grid point on the interface becomes less than the value of the isentropic information surface, then the quantities at that grid point are allowed to enter into the integration once again.

After an isentropic surface has plunged into the sigma-coordinate layer, then the values of velocity, pressure and Montgomery streamfunction are missing at the adjacent grid point on the warm side of the intersection complicating the calculation of finite differences along the isentrope. A simple linear extrapolation downward from the isentropic coordinate region is used to obtain the values at the grid point which has plunged into the sigma-coordinate region.

f. Folding isentropes

Numerical instability appears in the model when the value of the inverse stability $\gamma=-\Delta p/\Delta\theta$ approaches either zero or infinity in the isentropic coordinate region. Because an independent pressure tendency given by (6) is computed along each isentrope, there is a possibility that pressure could increase with potential temperature which would cause the value of γ to approach zero and then become negative as the integration proceeds onward in time. Isolated regions in which this type of instability occurs are observed in the atmosphere (Lilly and Toutenhoofd, 1969), but must be prevented from occurring in the numerical model because potential temperature is the vertical coordinate.

Another numerical problem that produces computational instability can occur when there is a strong upward flux of sensible heat in the boundary layer causing the value of potential temperature to increase along the coordinate interface. In this case the value of γ approaches infinity immediately before the potential temperature information surface intersects the top of the sigma-coordinate layer because the value of $\Delta\theta$ is decreasing toward zero.

For these reasons, the value of γ is never allowed to become less than 0.01 mb K^{-1} or greater than 300 mb K^{-1} during the simulation in the isentropic-coordinate region. At the completion of each time step, the predicted value of γ is calculated for each layer and compared to the range 0.01–300 mb K^{-1}. If the value of γ is outside these limits, then the value of pressure is altered slightly at the top of the layer to ensure that γ is within the prescribed range. This procedure conserves mass in each vertical column and subdues the incipient numerical instability before it becomes serious.

Because γ is always greater than zero in the isentropic-coordinate region of the model, the stratospheric rotors that are observed on the leeward side of mountain barriers in the actual atmosphere cannot occur in the model atmosphere. However, γ can become negative or infinite in the sigma-coordinate layer because in this layer potential temperature is a prognostic variable and the vertical coordinate is a function of pressure.

g. The boundary conditions

In any two-dimensional model, three requirements should be fulfilled at the upstream and downstream boundaries: 1) net mass flux through the system should vanish if the boundary conditions are not time dependent; 2) waves of any scale should be allowed to escape through both upstream and downstream boundaries and not be reflected back into the computational grid; and 3) the lateral boundary conditions should not be modified by perturbations generated within the computational region.

In a preliminary version of the present model, cyclic boundary conditions were utilized at the lateral boundaries. This type of lateral boundary condition, which is easily implemented and conserves mass and energy, proved to be unsatisfactory after a few trials. Unless the upstream boundary is far removed from the disturbance, waves generated by the phenomena being studied can propagate downstream and eventually reenter the grid at the upstream boundary. These reentering waves modify the upstream boundary condition and interact with the solution, thus producing unrealistic results.

The next lateral boundary conditions attempted were the open type in which the first horizontal derivative of all quantities is set equal to zero at inflow grid points and the second horizontal derivative of all quantities is set equal to zero at outflow boundaries. With these open boundary conditions, all variables can change with time at the boundaries as a result of the development of the disturbances within the interior. However, this boundary condition may be reasonable if the variations of quantities is described satisfactorily at the lateral boundaries.

This open boundary condition resolved the problem of waves reentering the grid and modifying the solution. However, another problem developed that completely dominated the solution after running the model a few hundred time steps. As the simulation proceeded farther along in time, the values of the thermodynamic variables at the lateral boundaries became unrealistic. Alternate layers of high stability and low stability appeared at the lateral boundaries which eventually changed the solution over the entire computational domain. Although the solution remained computationally stable throughout the entire time integration, this set of boundary conditions also had to be rejected.

After these tests it became apparent that a lateral boundary region had to be found that would allow waves to escape through the boundary, but not change the forcing at the boundaries. These criteria were met by expanding the grid spacing exponentially in the upstream and downstream directions, thus moving the lateral boundaries away from the region of interest. In addition, an artificial dissipation algorithm (described as a "computational sponge") designed to absorb small-scale perturbations was inserted between the interior domain and each lateral boundary which allows the conditions at the boundaries to remain constant in time.

The computational sponge is formed by varying the value of the horizontal diffusion coefficient. In the interior region of interest, the value of the diffusion coefficient is fixed at $0.02(\Delta x)^2/8\Delta t$, which damps 2% of the $2\Delta x$ wave each time step. In the buffer zones on either side of the central region, the value of the diffusion coefficient is increased linearly to a maximum value that damps 100% of the $2\Delta x$ wave as it nears each lateral boundary. This simple procedure prevents waves from reentering the grid and does not permit the forcing to change at the lateral boundaries.

Because sigma coordinates are used in the lower layer, the lower boundary condition is simply $d\sigma/dt=0$ along the surface ($\sigma=1$) at the surface of the earth.

For the boundary condition at the top of the model an idealized layer (Shuman and Hovermale, 1968) is assumed to extend from the last isentropic surface to infinity where the value of pressure is zero. Although no computations are made in this layer, a few assumptions lead directly to a pressure tendency equation which can be applied at the uppermost isentropic surface in the computational region. In this layer the vertical coordinate is

$$\sigma=p/p^{**}, \tag{27}$$

where p^{**} is the pressure along the uppermost surface ($\theta=\theta^{**}$). Because $d\sigma/dt=0$ along the surface ($\theta=\theta^{**}$), the equation of motion (6) becomes

$$\frac{\partial u^{**}}{\partial t}=-u^{**}\frac{\partial u^{**}}{\partial x}-\frac{\partial \psi^{**}}{\partial x}, \tag{28}$$

where the double superscript refers to quantities at the top of the model.

The continuity equation (14), after integration through the layer and substituting

$$\frac{\partial p}{\partial \sigma}=p^{**}, \tag{29}$$

becomes

$$\frac{\partial p^{**}}{\partial t}=-\int_0^1 \frac{\partial}{\partial x}(u^{**}p^{**})d\sigma. \tag{30}$$

With the additional assumption that there is no vertical wind shear or potential temperature gradient in this idealized quiescent layer, the pressure tendency is

$$\frac{\partial p^{**}}{\partial t}=-\frac{\partial}{\partial x}(u^{**}p^{**}), \tag{31}$$

which applies at the top surface of the computational region.

3. Experimental results and discussion

Because the major problems that appear in isentropic-coordinate models are directly related to the planetary boundary layer, a series of experiments that put particular emphasis on the boundary layer was designed and performed to test the proposed vertical coordinate scheme. The problems that arise as a result of boundary layer phenomena are caused either by surface heating or by topographic irregularities. In each case, isentropes intersect the surface of the earth. Moreover, for the surface heating case, the lapse rate can become equal to the adiabatic rate in the surface

layer. Simple experiments devoted separately to each of these phenomenon will be performed.

The first experiment tests the vertical coordinate scheme when the surface of the earth is irregular by simulating flow over a mountain. The amplitude, wavelength and position of the waves that develop during the flow over a mountain will be examined.

The second experiment is designed to show that the proposed vertical coordinate scheme can handle surface adiabatic layers which develop as a result of heating near the surface of the earth. An electrical power park is simulated by inserting a large temperature excess at the surface of the earth. The effect of this heat source on the model atmosphere is examined by calculating heat and momentum fluxes to evaluate the vertical transfer of these important quantities.

The fluxes were calculated by

$$\left.\begin{aligned}\text{momentum flux} &= \rho\overline{w'u'}\\ \text{heat flux} &= c_p\rho\overline{w'\theta'}\end{aligned}\right\}, \tag{32}$$

in which an overbar denotes an average along a constant height surface and primed quantities are deviations from the mean value of each height. The average was performed over the interior portion of the grid and did not contain the lateral boundary regions.

a. Flow over a mountain

In this experiment isentropic surfaces will be compelled to intersect the surface of the earth by dynamic forcing when the surface of the earth is not flat. An initial thermodynamic state and momentum field will be deformed by placing a symmetric barrier which resembles a mountain along the lowest surface of the model.

Clear air turbulence appears frequently in the stratosphere over mountain ranges and is usually associated with small-scale waves [wavelengths of 1–10 km (Lilly and Toutenhoofd, 1969)] that are superimposed on the larger scale forced waves. Because the grid increment in the numerical model is 7 km, these small-scale waves will not appear. However, waves with a wavelength comparable to the wavelength of the mountain range (30–50 km) should appear during the simulation.

The function chosen to represent the height of the mountain for the simulation was

$$z = hb^2/(x^2+b^2), \tag{33}$$

which forms a symmetric barrier of maximum elevation h and half-width b. Here x is the distance upstream or downstream from the center of the mountain. The parameters h and b were set equal to 1.9 km and 15 km which approximates the terrain of the Rocky Mountains to the west of Boulder, Colo.

In the present situation the surface elevation (33) is allowed to change slowly as a function of time to ensure that the initial conditions are free of accelerations. Hence, the lowest surface of the model is slowly transformed from the initial horizontal surface to a bell-shaped symmetric barrier. The time rate of change of the simulated diastrophism was determined by trial and error. If the barrier is introduced too fast, then the spurious accelerations and hydrostatic imbalances cause pertubations that are slowly removed by the diffusion and the implicit smoothing of the semi-momentum finite difference operators. Consequently, a quasi-steady-state solution is reached only after an excessive amount of computer time has elapsed. For this reason, the elevation of each grid point along the surface "grows" 1/180th of its maximum value each 20 s time step for the first 180 time steps. With this rate a quasi-steady-state solution is reached in about 1.5–2 h of model time after the mountain is in place. Thus, in the experiment to follow, the mountain is introduced during the first hour of simulation time and the results are displayed 2 h after the mountain has stopped growing.

A parameter that is used in linear wave theory to describe the flow over mountains was calculated to determine if the solutions obtained from the model described here resembled those obtained from linear models. If the critical wavenumber (Queney, 1948; Scorer, 1949)

$$K_c^2 = \frac{g}{\theta}\frac{\partial\theta}{\partial z}\Big/u^2 \tag{34}$$

or Scorer parameter is calculated from the initial conditions for the simulation of flow over a mountain, then the horizontal and vertical wavelengths of the forced waves that develop during the numerical simulation can be compared to those of the linear model.

The initial thermodynamic conditions for the experiment are the U. S. Standard Atmosphere and the initial wind profile is a constant 15 m s^{-1} at every grid point in the model. These initial conditions produced the critical wavenumber profile that is illustrated in Fig. 1.

The potential temperature distribution (Fig. 2) has been modified after 3 h of simulation from the original horizontal distribution of the isentropes to standing waves. The waves have a maximum peak-to-peak amplitude of about 2.5 km and tilt upstream over the mountain with increasing elevation. Tilted waves similar to these appear in the atmosphere whenever the flow is normal to a mountain and are responsible for the lenticular clouds commonly observed in the lee of the Rockies.

The critical wavenumber profile (Fig. 1.) has two distinct regions separated by the tropopause near 10 km which indicates that a linear model would produce lee waves with shorter wavelengths in the stratosphere than in the troposphere because the critical wavenumber is largest in the stratosphere. The distribution of the lee waves in Fig. 2 agrees qualitatively with the

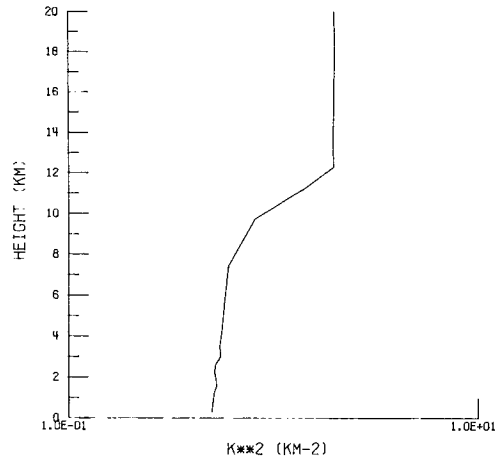

FIG. 1. The vertical profile of the critical wavenumber for the simulation of flow over a mountain.

wavelengths suggested by the critical wavenumber profile. The horizontal wavelength decreases from about 50 km in the troposphere to about 35 km in the stratosphere while the vertical wavelength decreases from 10 to about 4 km.

The horizontal wind speed (Fig. 3) has increased at the surface from the initial value of 15 m s^{-1} to greater than 36 m s^{-1} on the lee slop of the mountain. Strong winds are a common occurrence on lee slopes of the Rocky Mountains during late winter and early spring whenever the prevailing wind direction is out of the west. For example, a peak velocity of 60 m s^{-1} was recorded at the surface in Boulder, Colo., during the evening of 7 January 1969 (Danielsen and Bleck, 1970).

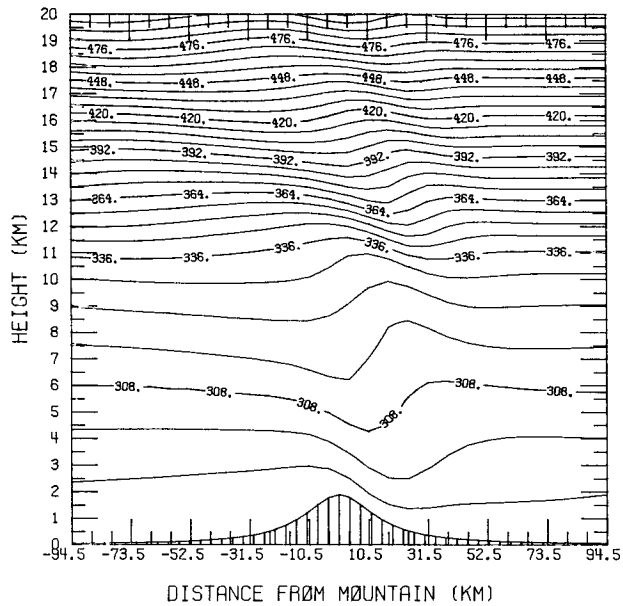

FIG. 2. The distribution of potential temperature (K) at $t=3$ h for the simulation of flow over a mountain.

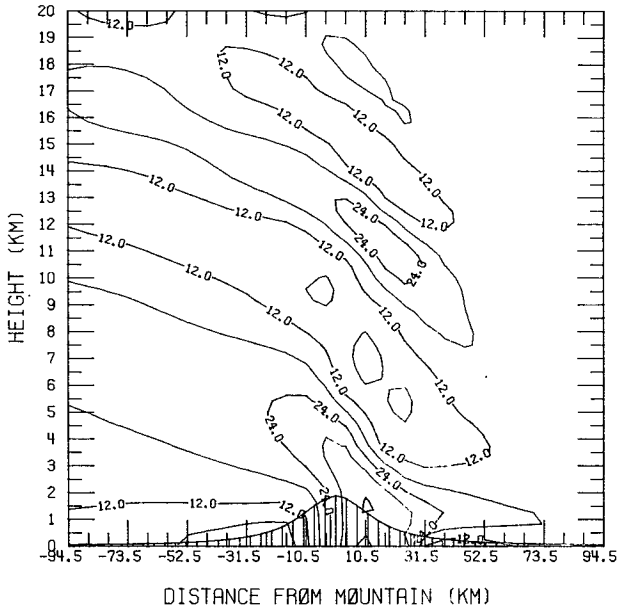

FIG. 3. As in Fig. 2 except for horizontal velocity (m s^{-1}).

Because the flow is blocked by the mountain on the windward side, the horizontal velocity has decreased to a value of 6 m s^{-1} at the surface in this region.

The vertical velocity (Fig. 4) is downward on the lee slope with a maximum velocity of -2.4 m s^{-1}. The tilted waves are prevalent in the vertical velocity pattern through the entire atmosphere. However, the amplitude of the waves is much weaker in the upper atmosphere than at the surface.

The momentum flux (Fig. 5) is downward everywhere with a maximum value of -33 dyn cm^{-2} appearing at

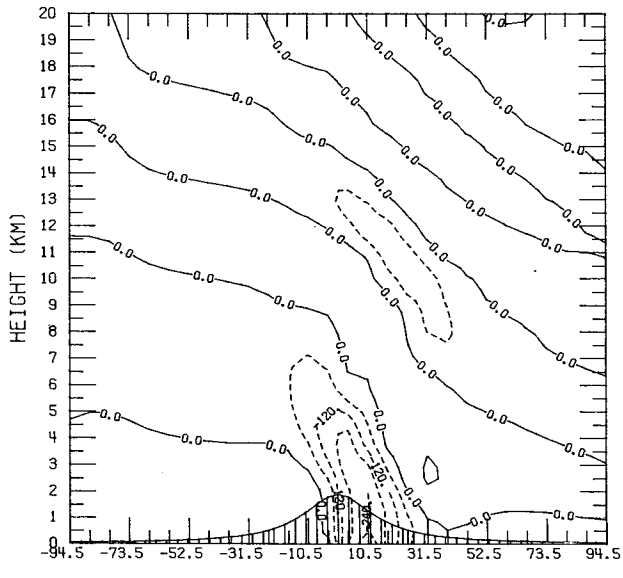

FIG. 4. As in Fig. 2 except for vertical velocity (cm s^{-1}).

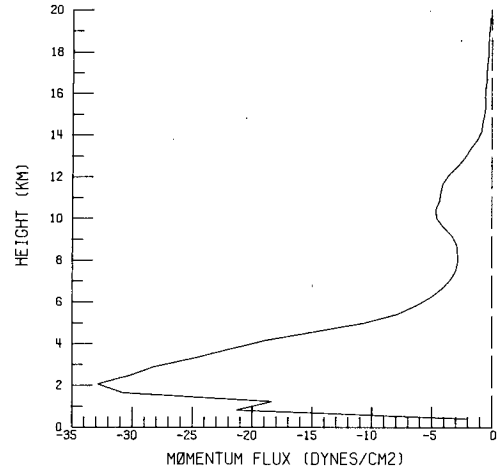

FIG. 5. The vertical profile of momentum flux.

an elevation of 2 km which is near the height of the mountain. Above the mountain, the flux profile has a positive slope indicating a region of momentum flux divergence which is caused by the large pressure gradient created by the flow over the surface barrier. Below mountain level the momentum is reduced by surface friction and the blocking effect of the mountain. For this reason, a negative slope or region of flux convergence appears in the flux profile between the surface and mountain height.

During the development of the model, a free top surface ($dp/dt=0$) was utilized as the upper boundary condition instead of the surface that is currently in use. In this case, the waves did not tilt with height and the velocity deviations u' and w' had zero correlation.

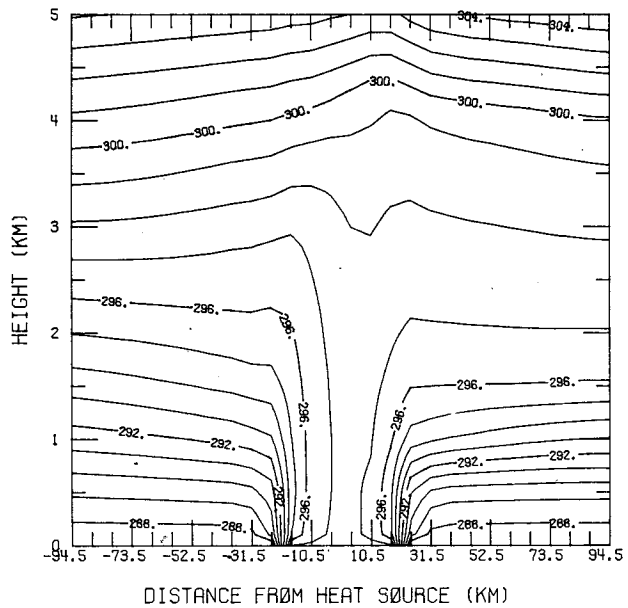

FIG. 6. The distribution of potential temperature (K) at $t=9$ h for the simulation of flow normal to a heat source.

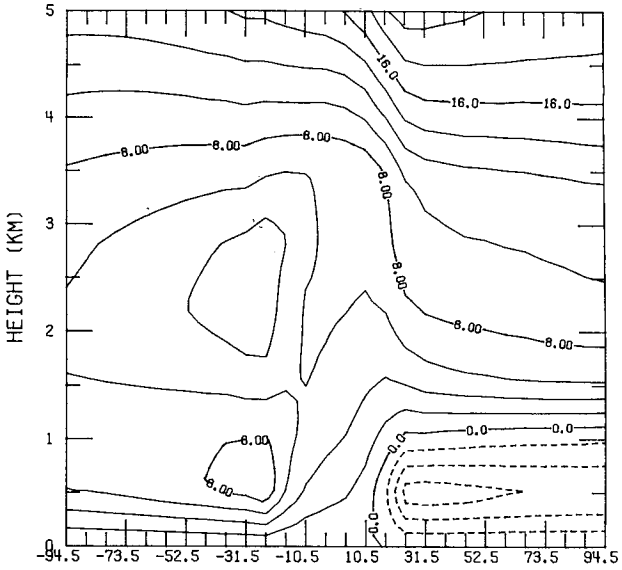

FIG. 7. As in Fig. 6 except for horizontal velocity (m s^{-1}).

Because the solution was in perfect quadrature, the momentum flux profile was zero everywhere.

This experiment has illustrated that the sigma-isentropic vertical coordinate system can be used to simulate atmospheric flow when the lower boundary is not horizontal. The coordinate interface did not inhibit or contribute to the transfer of momentum or heat during the simulation of lee waves. All of the variables maintained a smooth transition across the coordinate interface during the entire simulation.

b. Flow in response to surface heating

Because the model is two-dimensional, the model atmosphere is constrained to flow only in the vertical plane without turning or forcing in the direction normal to the cross section. Hence, the temperature excess at the surface will represent an infinite, homogeneous disturbance in the direction normal to the flow.

The temperature excess is introduced slowly as a function of time (0.25 K per 20 s time step) to inhibit the formation of Lamb waves that would appear if the entire 10 K temperature excess were introduced during one time step.

The initial thermodynamic state at each grid point in the model atmosphere is interpolated from the U. S. Standard Atmosphere. After an integration of the hydrostatic equations (5) and (12) in each coordinate system, the initial wind profile is determined by

$$u=\begin{cases}4z-0.2z^2, & 0\leqslant z\leqslant 20\text{ km}\\ 0, & z>20\text{ km}\end{cases} \tag{35}$$

where u is calculated in units of meters per second and z is measured in kilometers. Initially, at $t=0$, the wind

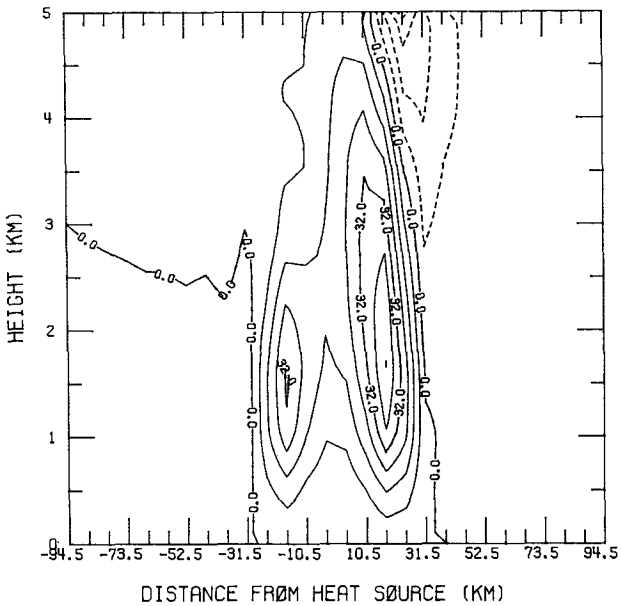

FIG. 8. As in Fig. 6 except for vertical velocity (cm s^{-1}).

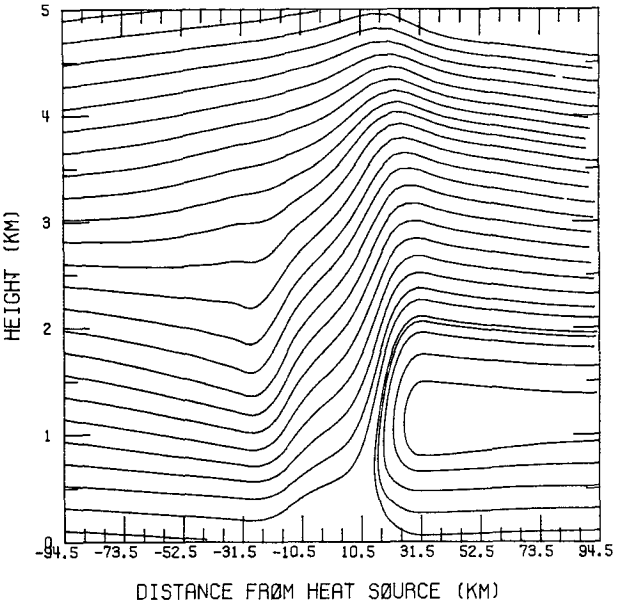

FIG. 9. The distribution of steady-state trajectories (streamlines) started at each lateral edge at $t=9$ h.

speed at every grid point in the model is determined by this procedure. However, as the integration proceeds forward in time, the equations of motion [(3), (9)] determine the wind speed at all interior grid points while the values at each lateral edge are held constant as calculated from (35).

The values of potential temperature and the horizontal and vertical velocities after 9 h of simulation are given in Figs. 6, 7 and 8 for the lowest 5 km of the model atmosphere. The redistribution of potential temperature from the initially horizontal isentropes indicates that the strong heat source at the center of the grid (6 grid points) has modified the boundary layer temperature structure producing an adiabatic region directly over the heat source to a depth of about 3 km. Above the adiabatic layer cooling has occurred which produces the upward bulges of the isentropes above 3 km.

The horizontal velocity (Fig. 7) has increased at a height of 0.5 km near the windward edge from the initial value of 2 m s^{-1} to a value of about 8 m s^{-1}. On the leeward edge of the heat source at the same height the flow has reversed and has attained a value of 6 m s^{-1} into the heated region. This region of strong convergence (4×10^{-4} s^{-1}) is causing cooler air to be advected from upstream and downstream into the region of heating at the surface. Near the surface of the earth the heating overtakes the advection of cooler air and a surface-based superadiabatic lapse rate develops.

Two cells of upward motion (Fig. 8) have developed near the lateral boundaries of the heat source. Mass conservation is maintained by a small downward velocity which is spread over a large area upstream and downstream from the heat source.

Trajectories (Fig. 9) constructed from the horizontal and vertical components of the velocity after a quasi-steady-state solution has been attained show the presence of the large diabatic heating when compared to the distribution of the isentropes (Fig. 6). The diabatic heating (Fig. 10) is a maximum at the lateral edges of the heat source at a height of 0.5 km which is near the region of maximum horizontal velocity and accounts for the sea breeze front that has been produced by the surface temperature excess.

The large vertical velocities over the surface temperature excess create a barrier to the horizontal flow

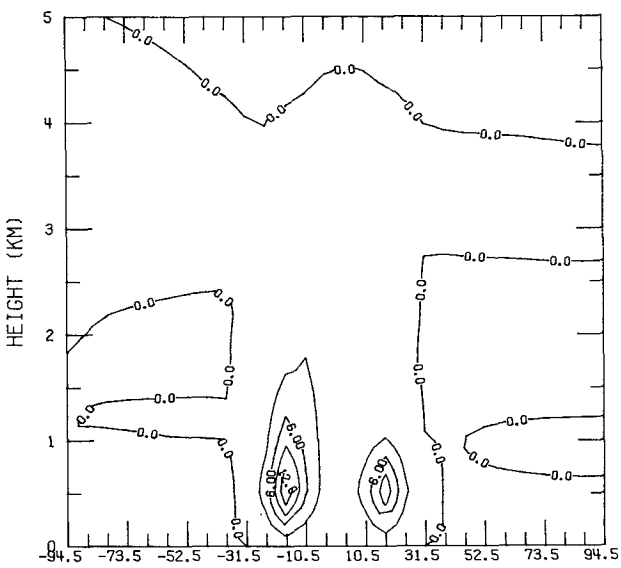

FIG. 10. The diabatic heating rate (K h^{-1}) at $t=9$ h.

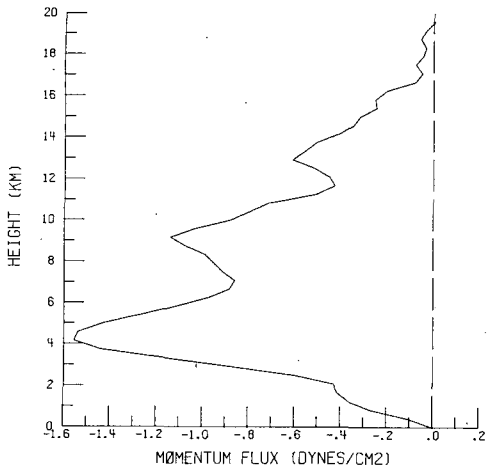

FIG. 11. The vertical profile of momentum flux at $t=9$ h.

that is similar to the topographic barrier in the previous experiment. Here a pressure gradient is induced by thermodynamic forcing rather than the mountain barrier. However, standing waves analogous to lee waves are formed as the flow responds to the thermodynamically induced obstruction.

The momentum flux (Fig. 11) is downward with the maximum downward flux appearing at a height of 4 km which represents the height of the effective barrier. Again, as in the previous experiment, there is a region of flux divergence above the 4 km barrier and a region of flux convergence below 4 km.

A strong upward heat flux of about 150 W m^{-2} appears at a height of 1 km in the heat flux profile (Fig. 12). The heat flux profile is a direct consequence of the surface temperature distribution and the parameterization scheme which has produced a downward or negative heat flux at about 3.5 km. The cooling along the 299 K isentrope (Fig. 6) is a result of this downward heat flux immediately above the adiabatic layer. In the actual atmosphere the mixing is enhanced

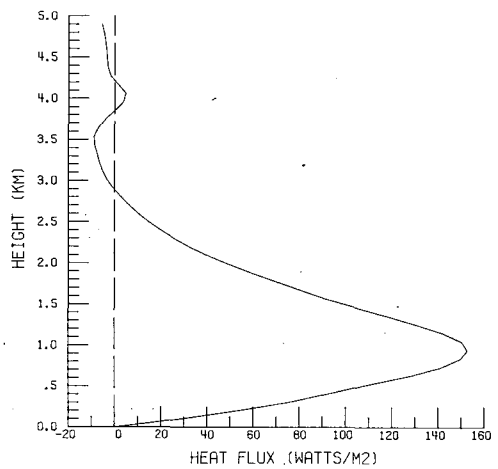

FIG. 12. The vertical profile of heat flux at $t=9$ h.

at the top of the well-mixed layer by penetrative convection in which the thermal overshoots into the inversion base and then subsides bringing momentum, heat and kinetic energy into the adiabatic layer. In the model atmosphere the downward flux at the top of the mixed layer is produced by the parameterization scheme which permits a countergradient heat flux. Heat flux profiles with a downward flux above the adiabatic layer have been observed in empirical studies (Telford and Warner, 1964) and have been verified in theoretical studies (Tennekes, 1973).

This experiment has demonstrated that the new sigma-isentropic vertical coordinate system described here can be utilized to simulate the effects of diabatic heating. The coordinate interface cannot be detected in any figures depicting the numerical results of the integration, and heat and momentum were transferred across the coordinate interface realistically.

4. Conclusion

A solution for the problems of modeling planetary boundary phenomena when potential temperature is utilized as the vertical coordinate in a primitive equation numerical model has been proposed and evaluated. The problem of isentropes intersecting the surface of the earth (or overturning when the lapse rate becomes adiabatic) is solved using a function of pressure as the vertical coordinate in the lower region of the model. In the vertical the model is subdivided into two distinct regions by a coordinate interface which is positioned in the lower troposphere above the planetary boundary layer. Although the potential temperature surfaces still intersect the interface surface, the intersection here appears to create no problems.

With this scheme the effects of surface heating can be simulated. Adiabatic and superadiabatic lapse rates can develop near the surface of the earth without destroying the vertical coordinate. An additional benefit gained from the coordinate transformation is the ease of incorporating complicated surface topographic features into the model because the vertical coordinate is a constant along the surface of the earth.

The ultimate test of this or any numerical model has to be the simulation and verification of the processes that occur in the complex three-dimensional atmosphere. The extension of the model developed here to three dimensions should be relatively easy and straightforward. However, an initialization scheme will have to be developed to permit actual atmospheric data rather than analytic functions to be used for the initial conditions. The three-dimensional initialization scheme would have to ensure that the initial mass and momentum fields are balanced within the sigma-isentropic vertical coordinate framework.

The separate tests that were performed here have shown that the problems appearing in isentropic-coordinate numerical models can be dealt with individually.

After the computer program for the model was completed, no parameters were changed other than the initial conditions. That is, the model was not "tuned" for each individual experiment. The same parameterization of the eddy diffusion coefficient was utilized for surface heating and flow over a mountain experiments.

With the present generation of computing machines ready to provide enough storage for a high-resolution boundary layer, the time has come to take advantage of the isentropic nature of atmospheric flow. It is now possible to use isentropic coordinates in numerical prediction models.

Acknowledgments. The author gratefully acknowledges the suggestions and constant encouragement given him by Professor John A. Dutton. Gratitude is also extended to Drs. J. B. Hovermale and E. F. Danielsen for their advice and assistance. This research was supported in part by the National Science Foundation under Grant GA1595X to the Pennsylvania State University.

REFERENCES

Danielsen, E. F., and R. Bleck, 1970: Tropospheric and stratospheric ducting of stationary mountain lee waves. *J. Atmos. Sci.*, **27**, 758–772.

Deardorff, J. W., 1967: Empirical dependence of the eddy coefficient for heat upon stability above the lowest 50 m. *J. Appl. Meteor.*, **6**, 631–643.

Deaven, D. G., 1974: A solution for boundary problems in isentropic coordinate models. Ph.D. dissertation, The Pennsylvania State University, 136 pp.

Eliassen, A., and E. Raustein, 1968: A numerical integration experiment with a model atmosphere based on isentropic coordinates. *Meteor. Ann.*, **5**, 45–63.

Haltiner, G. J., 1971: *Numerical Weather Prediction.* Wiley, 224–225.

Lilly, D. K., and W. Toutenhoofd, 1969: The Colorado lee wave program. *Clear Air Turbulence and its Detection*, Plenum Press, 232–245.

Pedlosky, J., 1964: The stability of currents in the atmosphere and the ocean. Part I. *J. Atmos. Sci.*, **21**, 201–219.

Queney, P., 1948: The problem of air flow over mountains: A summary of theoretical studies. *Bull. Amer. Meteor. Soc.*, **29**, 16–26.

Scorer, R. S., 1949: Theory of waves in the lee of mountains. *Quart. J. Roy. Meteor. Soc.*, **75**, 41–56.

Shuman, F. G., 1962: Numerical experiments with the primitive equations. *Proc. Intern. Symp. Numerical Weather Prediction* 7–13 November 1960, Meteor. Soc. Japan, 85–107.

——, and J. B. Hovermale, 1968: An operational six-layer primitive equation model. *J. Appl. Meteor.*, **7**, 525–547.

Telford, J. W., and J. Warner, 1964: Fluxes of heat and vapor in the lower atmosphere derived from aircraft observations. *J. Atmos. Sci.*, **21**, 539–548.

Tennekes, H., 1973: A model for the dynamics of the inversion above a convective boundary layer. *J. Atmos. Sci.*, **30**, 558–567.